[논 문] 한국재료학회지
Korean Journal of Materials Research
Vol. 7, No. 6 (1997)

고분해능 투과전자현미경을 이용한 $Pb(Mg_{1/3}Nb_{2/3})O_3$ 고용체의 미세구조 연구

박 경 순
충주산업대학교 재료공학과

Microstructural Studies of $Pb(Mg_{1/3}Nb_{2/3})O_3$ Solid Solutions by High-resolution Transmission Electron Microscopy

Kyeongsoon Park
Department of Materials Engineering, Chung-ju National University, Chungju, Chungbuk 380-702

(1997년 2월 1일 받음, 1997년 4월 21일 최종수정본 받음)

초 록 고분해능 전자현미경과 컴퓨터 이미지 시뮬레이션이 La이 첨가되고 또한 첨가되지 않은 $Pb(Mg_{1/3}Nb_{2/3})O_3$ 고용체의 미세구조를 연구하기 위해서 사용되었다. 불규칙격자 영역과 규칙격자 영역의 격자 이미지는 정방정 형태와 유사 육방정 형태를 각각 보였다. 규칙격자 영역에서 Mg과 Nb의 비화학양론적인 규칙격자 구조 현상이 〈111〉방향에 따라 관찰되었다. 실험 격자 이미지와 컴퓨터 시뮬레이션 이미지의 비교로부터, 규칙격자 구조를 가지는 영역의 장거리 규칙도는 0.2~0.7의 값을 가지고 있었고, 또한 규칙격자는 $(NH_4)_3FeF_6$ 결정구조를 가지고 있었다. 작은 값의 장거리 규칙도를 가지는 규칙격자를 가지는 영역에서, 변형률 파형이 〈111〉방향에 따라 관찰되었다. 이 변형률 파형은 〈110〉방향에 따라 B-위치에 있는 Mg과 Nb의 두 양이온이 그들의 위치로부터 변위 되었기 때문에 일어났다. 한편, 큰 값의 장거리 규칙도를 가지는 규칙격자를 가지는 영역에서, 변형률 파형이 관찰되지 않았다. 이것은 대부분 두 양이온이 그들의 위치에 있기 때문에, 원자 변위가 없었기 때문이다.

Abstract High-resolution transmission electron microscopy and computer image simulation were performed to investigate the microstructure of undoped and La-doped lead magnesium niobate solid solutions. The lattice images of disordered and ordered regions showed the tetragonal and pseudo-hexagonal patterns, respectively. The nonstoichiometric ordering of Mg and Nb cations in ordered regions was observed along the 〈111〉directions. By comparing the experimental and simulated lattice images for the ordered regions, it was determined that the long-range order parameter approximately range 0.2 to 0.7 and the ordered structure corresponds to a $(NH_4)_3FeF_6$ structure. For the ordered regions with a small value of the order parameter, the strain waves were observed along the 〈111〉directions. This strain modulation arises due to a displacement of Mg and Nb cations on two distinct B-site sublattices from their original positions along the 〈110〉directions. On the other hand, for the ordered regions with a high value of the order parameter, no strain waves were observed, since most cations are occupied at their specific B-site sublattices and thus suppress the atomic displacement.

1. INTRODUCTION

Lead-based ferroelectric compounds, $Pb(B^{I}_{x}B^{II}_{1-x})O_3$, with a cubic perovskite structure exhibit a high dielectric constant, a relatively low firing temperature, and a diffuse ferroelectric-paraelectric phase transition[1~3]. The diffuse phase transition is largely influenced by the degree in which the B-site atoms are ordered on the B-site sublattice. Ordering in $Pb(Mg_{1/3}Nb_{2/3})O_3$ (PMN) has been suggested to arise due to a compositional segregation, resulting in some regions being Mg-enriched[4~7]. The distribution of two kinds of B-site cations, Mg and Nb, on equivalent crystallographic positions causes a statistical composition fluctuation, forming microdomains with different Curie temperatures which contribute to a broad phase transition through a wide temperature range.

Several investigators have studied the ordered structure of the PMN and modified PMN ferroelectric relaxors by X-ray diffraction[8,9], TEM dark field imaging[2,10,11], and high-resolution transmission electron microscopy (HRTEM)[12~14]. However, no detailed information on the microstructure of the ferroelectric relaxor, especially ordered structure, has not been reported. In this work, detailed microstructure of undoped and La-doped PMN was investigated by high-resolution lattice imaging and computer image simulation.

2. EXPERIMENTAL

Undoped and La-doped PMN samples were prepared by the precalcination method[15]. La was added to increase the size of the ordered domains and the degree of

ordering. This is because the donor doping with La on the Pb-sites decreases the charge imbalance between the ordered and disordered regions[2]. MgO and Nb_2O_5 were prereacted to form columbite, and then milled with the appropriate proportions of PbO and La_2O_3. The samples for HRTEM were prepared by mechanical grinding, dimpling, and then ion-milling at liquid nitrogen temperature. The ion-milling was done using 4.5keV Ar^- ions and 1mA current in order to minimize ion-induced damage. The microstructure was investigated using a Jeol 2000FX-II transmission electron microscope operated at an accelerating voltage of 200keV.

To find the order parameter of ordered regions, the experimental lattice images of ordered regions were compared with simulated lattice images. Computer image simulations were performed using the multislice method[16~18] and undoped PMN on the assumption that the ordered structure corresponds to $(NH_4)_3FeF_6$ structure with allowance for factors such as specific composition and occupancy of the cations on the B-site sublattice, sample thickness, and microscope imaging conditions. In order to remove the noise in the experimental lattice images of the ordered regions, the experimental lattice images were digitized by the "Java" software, Fourier transformed, and then image processed by the "Semper 6" software.

3. RESULTS AND DISCUSSION

Figure 1 shows the (110) selected area diffraction (SAD) pattern from undoped PMN. In addition to (strong) allowed reflections originating from the cubic perovskite structure, extra (weak) superlattice reflections, marked by arrows, appear at positions $(h+\frac{1}{2}, k+\frac{1}{2}, l+\frac{1}{2})$ with respect to the fundamental reflections of the primitive perovskite unit cell ($a_0 \approx 0.402$nm). The existence of these superlattice reflections can be explained by the fact that there are some regions with ordered structure caused by the doubling $(2a_0 \times 2a_0 \times 2a_0)$ of the primitive perovskite unit cell.

Figure 2 shows a $\frac{1}{2}(1\bar{1}1)$ dark field image of 5% La-doped PMN. This figure shows that the ordered microdomains (bright areas) were embedded in a disordered region. Some of the ordered microdomains are indicated by arrows. The size of ordered microdomains is approximately in the range of 4 to 20nm. This ordered microdomains originated from a doubling $(2a_0 \times 2a_0 \times 2a_0)$ of the primitive perovskite unit cell ($a_0 = 0.402$nm). The formation of ordered regions reduces the elastic strain energy and electrostatic energy of the lattice that originate from the random distribution of the Mg and Nb cations with different sizes and charges among the octahedral sites. The driving force for ordering increases as the size and valence difference between two B-site cations is increased[19]. It was found that the size of the ordered domains increased with increasing the contents of the dopant La in PMN. This result is consistent with that by Chen *et al*[2]. and Lin *et al*[9].

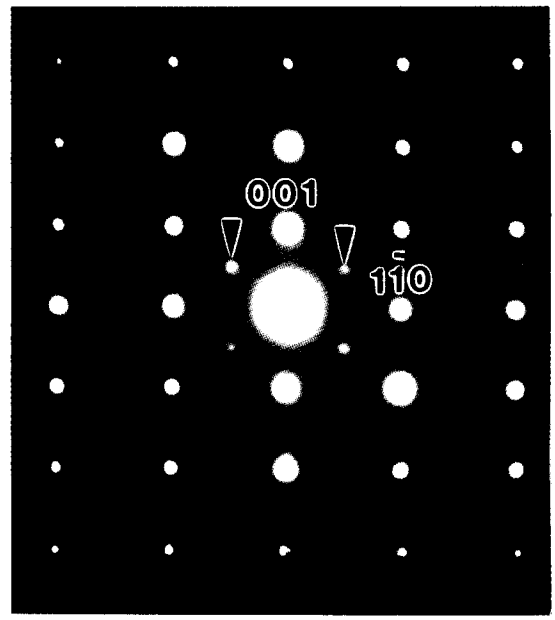

Fig. 1. (110) SAD pattern from undoped PMN. Two superlattice reflections are marked by arrows.

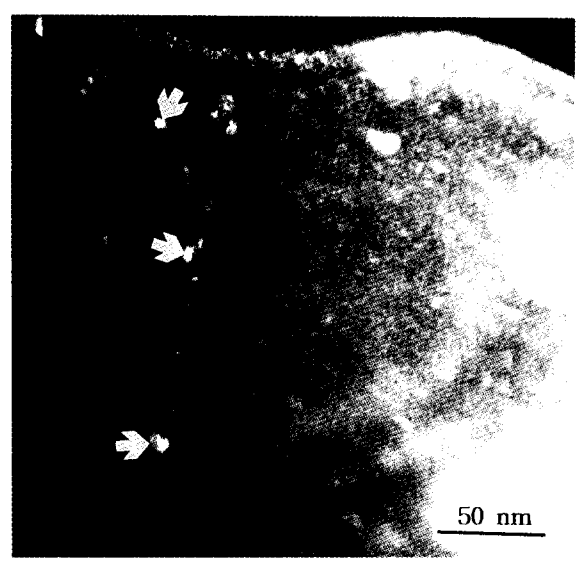

Fig. 2. $\frac{1}{2}(1\bar{1}1)$ dark field image of 5% La-doped PMN.

In order to investigate the microstructure of the ordered and disordered regions for undoped and La-doped PMN at the atomic level, experimental lattice images in the [110] projection were obtained under vari-

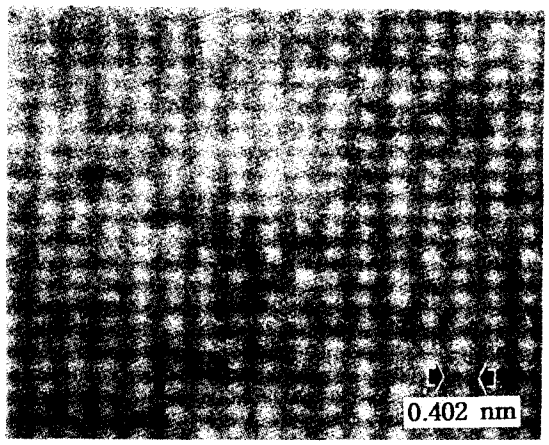

Fig. 3. High-resolution (110) lattice images of disordered regions obtained under an objective aperture with radius of 3.37 nm^{-1}.

ous microscope imaging conditions and objective apertures. The lattice images of disordered regions showed tetragonal patterns, as shown in Fig. 3. The same tetragonal pattern was observed from disordered regions, regardless of the objective aperture size, sample thickness, and defocusing value.

The experimental (110) lattice images from an ordered region under two different defocusing values and objective aperture with radius of 3.37nm^{-1} for 5% La-doped PMN are shown in Figs. 4(a) and (b). In addition to the (001) and (110) lattice fringes, a contrast modulation along the ⟨111⟩directions is clearly observed. The wavelength of the contrast modulation is ~ 0.464 nm, which corresponds to twice the calculated (111) interplannar spacing, strongly implying that the ordered structure arises due to a doubling of the perovskite unit cell. The long-range order parameter of the ordered region shown in Fig. 4 can be estimated by comparing the experimental images with the simulated images. The insets to Figs. 4(a) and (b) show the simulated images under defocusing values of −64 and −76nm, respectively, for a sample thickness of 12.5nm, objective aperture with radius of 3.37nm^{-1}, Mg : Nb ratio of 1 : 1, and long-range order parameter of 0.6. In Figs. 4(a) and (b), the experimental images are well matched with the simulated images.

The experimental (110) lattice images from different ordered region of 5% La-doped PMN under two different defocusing values of the objective lens and objective aperture with radius of 6.05nm^{-1} are shown in Figs. 5 (a) and (b). Contrast fluctuations, indicative of the ordered structure, are observed in Fig. 5(a), while no contrast fluctuations are observed in Fig. 5(b), even though both images were obtained from the same ordered region. The lattice image shown in Fig. 5(b) closely resembles that of the disordered regions (see Fig. 3). The insets to Figs. 5(a) and (b) show the simulated images under defocusing values of −88 and −100nm, respectively, for a sample thickness of 12.5nm, objective aperture with radius of 6.05nm^{-1}, Mg : Nb ratio of 1 : 1, and long-range order parameter of 0.2. The experimental and simulated images shown in Figs. 5(a) and (b) are well matched.

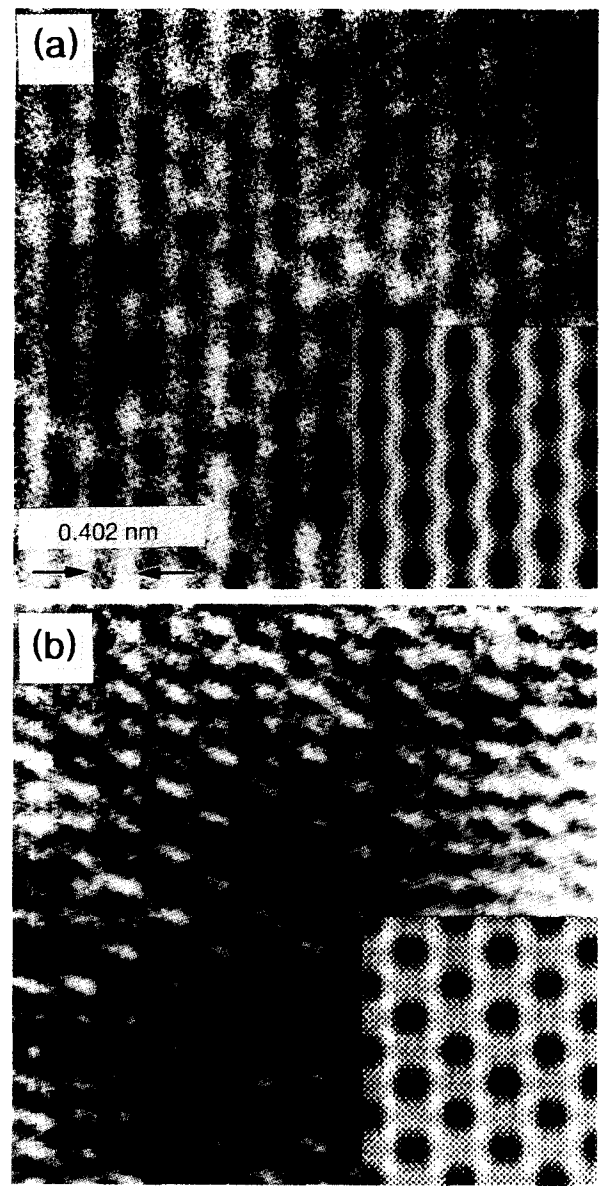

Fig. 4. High-resolution (110) lattice images from an ordered region under two different defocusing values and objective aperture with radius of 3.37nm^{-1} for 5% La-doped PMN.

The comparisons of the experimental and simulated images suggest that the value of the long-range order parameter varied between 0.2 and 0.7 and also the nonstoichiometric ordering of Mg and Nb cations occurred along the ⟨111⟩ directions. In the simulated im-

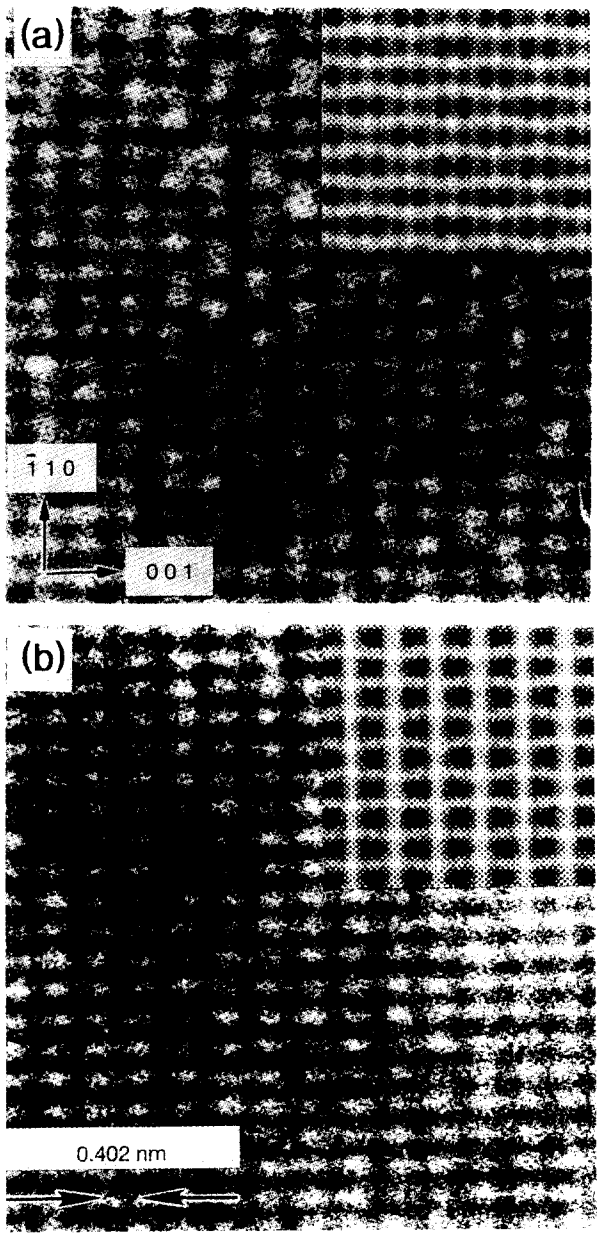

Fig. 5. High-resolution (110) lattice images from different ordered region of 5% La-doped PMN under two different defocusing values of the objective lens and objective aperture with radius of 6.05nm^{-1}.

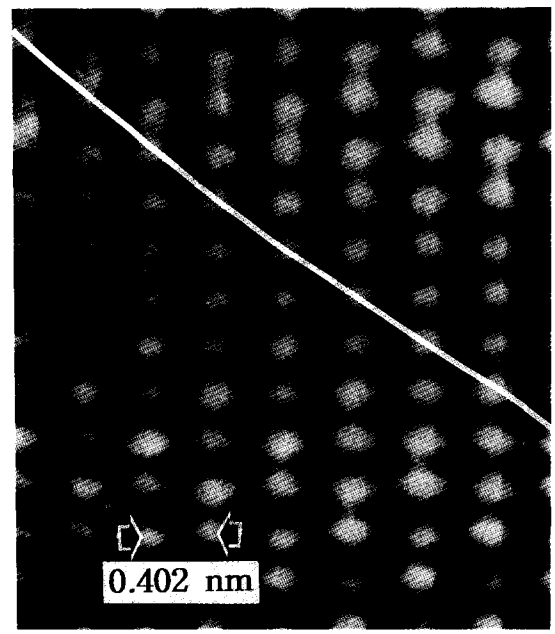

Fig. 6. Processed lattice image of the experimental lattice image shown in Fig. 5(a).

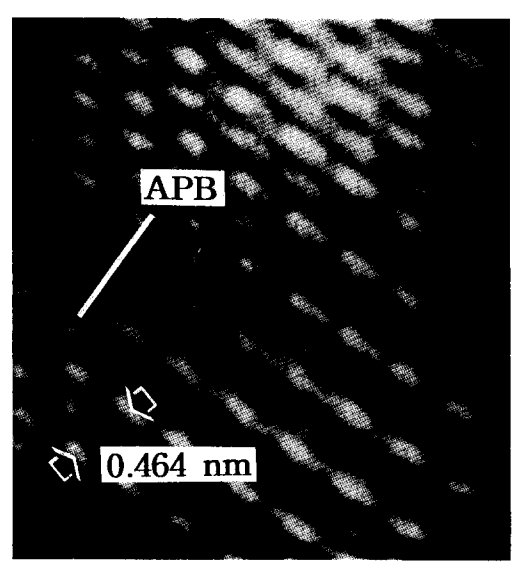

Fig. 7. Processed (110) lattice image from an ordered region of 5 % La-doped PMN.

ages, the complete ordered structure had a pseudo-hexagonal pattern. With decreasing the order parameter, the patterns changed slowly from a pseudo-hexagonal pattern to a rectangular pattern. The complete disordered structure had a rectangular pattern. It is not necessary that the local Mg : Nb ratio varies from 1 : 1 to 1 : 2 between the ordered and disordered regions. In addition, from the comparisons, it is apparent that the proposed model of $(NH_4)_3FeF_6$ structure for the ordered structure of PMN is valid.

The noise present in the experimental image shown in Fig. 5(a) was filtered by image processing. The processed lattice image is shown in Fig. 6. A network of larger and smaller dots representing the projections of the larger MgO_6 and smaller NbO_6 octahedra[8], respectively, is observed. A careful inspection of Fig. 6 shows that the (001) planes are displaced towards and away from each other along the [110] direction, thus giving rise to the distortion of neighboring MgO_6 and NbO_6 octahedra along this direction and the formation of (111) -polarized transverse strain waves[20]. The atomic displacement is because one sublattice is not occupied by its specific cation. The strain wave can be seen by looking down the line inside Fig. 6. This is the first observa-

tion that the ordered structure of PMN exist in a distorted perovskite polymorph. Consequently, the small NbO_6 octahedra residing in both sublattices can be nearest neighbors, causing a local expansion along the [110] direction. Bonneau *et al*[8]. has previously reported concurrent (110), (111), and (100) distortions from X-ray diffraction.

Figure 7 shows the processed (110) lattice image from an ordered region of 5% La-doped PMN. A contrast modulation along the ⟨111⟩directions, indicative of an ordered structure, is observed in Fig. 7. In this figure, any displacements of B-site cations from their original position and strain waves are not observed, since most cations are occupied at their specific B-site sublattices, thus suppressing the atomic displacement. An anti-phase boundary (APB) between two ordered microdomains is observed in Fig. 7, where a shift in the sequence of the (111) planes of Mg and Nb cations takes place. It is also important to note that the boundary between ordered and disordered regions is coherent, suggesting that there is no appreciable change in the lattice constant between these two regions other than a doubling of the perovskite unit cell. The disordered region is seen in the top area of Fig. 7.

4. CONCLUSIONS

The high-resolution lattice images of disordered regions for undoped and La-doped lead magnesium niobate solid solutions showed the tetragonal patterns, while the lattice images of ordered regions showed the pseudo-hexagonal patterns. The nonstoichiometric ordering of Mg and Nb cations in ordered regions occurred along the ⟨111⟩directions, giving rise to a doubling of the primitive perovskite unit cell. From the extensive visual comparisons of the experimental and simulated images, the ordered regions had a $(NH_4)_3FeF_6$ structure and also the order parameter in ordered regions was in the range of 0.2 to 0.7.

In addition, strain waves were observed in the ordered regions with a small value of the order parameter along the ⟨111⟩directions. These strain waves arise due to a displacement of Mg and Nb cations on two distinct B-site sublattices from their original positions along the ⟨110⟩directions. This displacement is because one sublattice is not occupied by a specific cation. On the other hand, no strain waves were observed in ordered regions with a high value of the order parameter, since most cations are occupied at their specific B-site sublattices, thus suppressing the atomic displacement.

REFERENCES

1. T. R. Shrout and A. Halliyal, Amer. Ceram. Soc. Bull., **66**, 704 (1987).
2. J. Chen, H. M. Chan, and M. P. Harmer, J. Amer. Ceram. Soc., **72**, 593 (1989).
3. A. S. Bogatin, A. A. Bokov, I. P. Rayevsky, and V. P. Filippenko, Ferroelectrics, **108**, 232 (1990).
4. U. K bler and K. Binder, J. Magn. Magn. Mater., **15-18**, 313 (1980).
5. D. H ser, L. E. Wenger, A. J. Van Duyneveldt, and J. A. Mydosh, Phys. Rev., **B27**, 3100 (1983).
6. G. A. Smolenskii, J. Phys. Soc. Jpn., **28**, 26 (1970).
7. L. E. Cross, Ferroelectrics, **76**, 241 (1987).
8. P. Bonneau, P. Garnier, E. Husson, and A. Morell, Mater. Res. Bull., **24**, 201 (1988).
9. L. J. Lin and T. B. Wu, J. Amer. Ceram. Soc., **73**, 1253 (1990).
10. A. D. Hilton, D. J. Barber, C. A. Randall, and T. R. Shrout, J. Mater. Sci., **25**, 3461 (1990).
11. A. D. Hilton, C. A. Randall, D. J. Barber, and T. R. Shrout, Ferroelectrics, **93**, 379 (1989).
12. H. B. Krause, J. M. Cowley, and J. Wheatley, Acta Crystallogr., **A35**, 1015 (1979).
13. E. Husson, M. Chubb, and A. Morell, Mater. Res. Bull., **23**, 357 (1988).
14. Z. C. Kang, C. Caranoni I. Siny, G. Nihoul and C. Boulesteix, J. Solid State Chem., **87**, 308 (1990).
15. S. L. Swartz and T. R. Shrout, Mater. Res. Bull., **17**, 1245 (1982).
16. J. M. Cowley and A. F. Moodie, Acta Crystallogr., **10**, 609 (1957).
17. J. M. Cowley and A. F. Moodie, Acta Crystallogr **12**, 353 (1959).
18. J. M. Cowley and A. F. Moodie, Acta Crystallogr **12**, 360 (1959).
19. M. P. Harmer, J. Chen, P. Peng, H. M. Chan, and D. M. Smyth, Ferroelectrics, **97**, 263 (1989).
20. D. Viehland, private communication.